Sixth International Symposium on Turbulence and Shear Flow Phenomena
Seoul, Korea, 22-24 June 2009

NUMERICAL STUDIES OF A HIGHLY ANISOTROPIC RECIRCULATION BUBBLE IN A THIN FLAT PLATE AT SMALL ANGLE OF ATTACK

André Luiz T. Rezende
arezende@aluno.puc-rio.br

Luiz Eduardo B. Sampaio
luizebs@esp.puc-rio.br

Angela O. Nieckele
nieckele@puc-rio.br

Department of Mechanical Engineering,
Pontifícia Universidade Católica do Rio de Janeiro – PUC/Rio
22453-900, Rio de Janeiro, RJ, Brazil

ABSTRACT

One of the situations that evidences some fundamental weakness of Reynolds Average Navier Stokes (RANS) approach to turbulence modeling is that involving highly anisotropic turbulence structures, such as that observed in long and thin recirculation zone in a high Reynolds number aerodynamic flow. Previous numerical studies tried to reproduce the experimental results from Crompton (2001) for a leading-edge separation in a thin flat plate at small incidence, using several RANS models. None of these models proved to be able of capturing some very important features of this flow, and it was suggested that Large-Eddy Simulations would not only provide more accurate results, but also allow a better physical understanding of the turbulence mechanisms. Therefore, in this work Large-Eddy Simulations is employed to determine the flow field over a thin flat plate, and results are compared with experimental data from Crompton (2001), with two completely different approaches for subgrid modeling: the traditional Dynamic Smagorinsky model from Germano (1999), and a new one, based on an advective forcing approach (Sampaio et al, 2007). Both approaches showed a very good agreement with the experimental data, and were able to capture all the important structures, such as boundary layer separation and reattachment, relaminarization, primary and secondary recirculation zones, and fast shear layer transition.

INTRODUCTION

The understanding of the flow around thin flat plate at shallow incidence can help in the design of airfoils and sails (Cyr and Newman, 1996), as well as flexible wing-based micro air vehicles (Lian and Shyy, 2005). The flow around an inclined flat plate with a sharp leading edge, as shown in Fig. 1, has a stagnation point located in its inferior surface, which results in a long and thin recirculation zone in the upper surface, denominated a thin airfoil bubble (Gault, 1957). The boundary layer around the leading edge is very thin, and it is expected to separate immediately, due to the flow direction change. The fixed separation point leads to the hypothesis that the flow will be insensitive to a change in Reynolds number, and transition will occur soon after separation.

The thin aerofoil bubble created on a plate with a sharp leading edge is therefore characterized by a flow separation

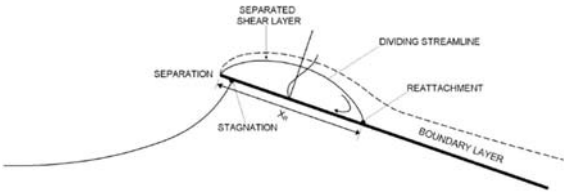

Figure 1: General flow around a thin flat plate at a small angle of attack.

at the leading edge with a reattachment to the upper surface at a point which moves gradually downstream with increasing incidence angle. As shown in Fig. 1, there is a dividing streamline which separates the bubble from the outer flow and which rejoins the surface at the reattachment point. For greater angles, usually above 7 degrees, there is no reattachment point, and the bubble enlarges downstream into the wake (Newman and Tse, 1992). Subsequent to separation, a deficiency of viscous damping at the wall means that the shear layer is expected to suffer transition very close to the leading edge. The turbulent shear layer increases quickly and has a high entrainment rate; it then reattaches further downstream and bifurcates. Part of the flow is directed to upstream to feed the shear layer. The resultant backflow reduces the pressure at the surface and in turn helps to bend the shear layer back to the reattachment point. The remaining flow is driven directed downstream where it gradually reverts to an attached turbulent boundary layer before reaching the trailing edge.

This complex flow around a plate at shallow incidence has been experimentally investigated by Crompton (2001), for the plate geometry shown in Fig. 2. Detailed velocity and turbulence statistics were measured in wind tunnel with Laser Doppler Anemometry (LDV) for incidence angles varying from 1 to 5 degrees. The Reynolds number based on the chord was 2.13×10^5.

Figure 2: Thin flat plate geometry.

Following the work of Crompton, numerical studies based on Reynolds Average Navier-Stokes methodology (RANS) with the $k\omega$ and $k\omega$-SST models were developed by Collie et al. (2008) and by Rezende and Nieckele (2007). Due to the inability of Reynolds Average models (RANS) to capture the strong anisotropy of this type of flow, this work presents the Large-Eddy Simulation (LES) methodology applied to the same thin flat plate test case, with an incidence angle of one degree, aiming a better understanding of the physics involved. Two different approaches to determined the subgrid effect on the large structures were employed and are described in the next section.

SUBGRID MODELING

The spatially-filtered Navier Stokes for an incompressible flow can be written as:

$$\frac{\partial \overline{\mathbf{u}}}{\partial t} + \nabla\cdot(\overline{\mathbf{u}}\,\overline{\mathbf{u}}) + \nabla\cdot\boldsymbol{\tau}_{\mathrm{SGS}} = -\nabla\overline{p}/\rho + \nu\nabla^{\mathbf{2}}\overline{\mathbf{u}}\,; \quad \nabla\cdot\overline{\mathbf{u}} = \mathbf{0}\,, \quad (1)$$

where $\overline{\mathbf{u}}$ and $\overline{p}$ are the filtered velocity and pressure, ρ and ν are the density and viscosity. The subgrid tensor is the result of commuting the filtering with the outer product and is defined as $\boldsymbol{\tau}_{\mathrm{SGS}} = \overline{\mathbf{u}\,\mathbf{u}} - \overline{\mathbf{u}}\,\overline{\mathbf{u}}$. A closed expression cannot be found for this subgrid tensor, and hence it must be separately modeled.

In eddy-viscosity models, which are designed to capture the forward energy cascade, attenuation is provided by an additional dissipative term. This is usually achieved by modeling the trace-free subgrid tensor

$$T_{\mathrm{SGS}_{ij}} = \tau_{\mathrm{SGS}_{ij}} - 1/3\ \tau_{\mathrm{SGS}_{kk}}\ \delta_{ij} \quad (2)$$

as

$$T_{\mathrm{SGS}_{ij}} = -2\ \nu_{\mathrm{SGS}}\ \overline{S}_{ij} \quad ; \quad \overline{S}_{ij} = 0.5\left(\frac{\partial \overline{u}_i}{\partial x_j} + \frac{\partial \overline{u}_j}{\partial x_i}\right), \quad (3)$$

where ν_{SGS} is the so-called subgrid viscosity and $\overline{S}_{ij}$ is the filtered strain rate.

In eddy-viscosity models, the success of a LES simulation depends mainly on the choice of the dissipative coefficient ν_{SGS}, which should provide just enough dissipation to damp the smallest modes, without overdamping other structures that might be important, either because they carry a significant percentage of the total turbulent energy, or because they play a significant role in the formation of other structures. In this context, an eddy-viscosity subgrid model with a feedback control mechanism is highly desirable, such as the dynamic approach proposed by Germano et al. (1991). In Germano's approach, the subgrid dissipation is decreased when the smallest modes are very weak and increased when they become important. The dynamic model was originally proposed as a way to automatically adjust the coefficient present in the Smagorinsky subgrid model (Smagorinsky, 1963), and to optimize it for different flow regimes. Such a dynamic approach can, in principle, be applied to any other model. In Germano (1999) it was shown that the model could be interpreted as a control feedback mechanism that forces the smallest resolved modes to have a fixed percentage of the energy contained in the intermediate range of the spectrum.

Apart from suffering from numerical instability (Sagaut, 2002), the dynamic model is still somewhat sensitive to mesh anisotropy, but this is the case for all eddy-viscosity approaches.

An alternative proposal for subgrid modeling, referred as "f-LES" (Sampaio et al, 2008), was employed in the present work. This subgrid model is based on a completely different representation of the small-large scales interaction, this time using an advective instead of a diffusive process to provide the adequate damping to a limited range of the spectrum. The sub-grid force $\mathbf{f}_{\mathrm{SGS}} = \nabla\cdot\boldsymbol{\tau}_{\mathrm{SGS}}$ is directly modeled, such that the smallest modes supported by the mesh are severely damped, while those with twice or more than twice their wavelength are almost or completely untouched. It is also a dynamic model as in Germano et al. (1991), in the sense that undesirable modes are detected and dampened.

A potentially advantageous effect of damping small modes is that the resulting discrete dynamic system is more robust and less prone to numerical instability. Since instability issues are often related to constraints not allowing the use of a regular mesh, the above mentioned effect is quite handy, allowing more flexibility in mesh design.

Dynamic Smagorinsk model

The sub-grid viscosity is modeled based on the Smagorinsly-Lilly Model (Samgorinsky, 1963), where the eddy-viscosity is modeled by

$$\nu_{\mathrm{SGS}} = \rho {L_s}^2 |\overline{S}| \quad ; \quad |\overline{S}| = \sqrt{2\overline{S}_{ij}\overline{S}_{ij}} \quad (4)$$

where L_s is the mixing length for subgrid scales

$$L_s = min(k\ d, C_s \forall^{1/3}) \quad (5)$$

and k is the von Krmn constant, d is the distance to the closest wall, C_s is the Smagorinsky constant and $\forall$ is the volume of the computational cell. In the dynamic approach, the Smagorinsky constant C_s is dynamically computed based on the information provided by the resolved scales of motion. Although, C_s can vary in time and space, to avoid instability it was clipped at zero and 0.23.

Advective formulation methodology

Following the general requirements for a good LES subgrid model, the derivation of this advective approach is split in three main steps. In order to be able to selectively damp only the very smallest modes supported by the mesh, firstly, a cut-off mode detector is derived, which will signal the presence of the smallest modes that the mesh scan represent and that must be damped. Secondly, using this detector as the basic element, we build a forcing term so that the appropriate damping rate is applied to these cut-off modes. Finally, further enhancements to the detector and forcing term to improve wave number selection and rate tuning.

The subgrid forcing term to be added to the filtered Navier-Stokes equation (Eq. 1) can then be written as:

$$\mathbf{f}_{\mathrm{SGS}} = \xi \mathbf{U}^* \cdot (\nabla \mathbf{U})^*\,, \quad (6)$$

where U^* is a characteristic velocity, $\mathbf{f}_{SGS}$ is a characteristic velocity gradient and ξ is a switch to improve frequency selectiveness.

The characteristic gradient part is actually the small modes detector, or cut-off detector, and can be based on a difference between two ways of calculating the gradients, corresponding to two different levels of accuracy. The idea is that the derivatives are stronger at the smallest mode that the mesh can represent, and the accuracy of the approximation will make a difference in this case. On the other hand, for modes whose wavelength is much greater than that of the cut-off mode, a low level approximation for the derivative would be already enough, and certainly very similar

to the high level approximation. Therefore, if the field is smooth, there would be no contents of the smallest mode, and both gradients (low level and high level approximations) would be similar, and their difference will be close to zero.

The velocity characteristic is just taken as the resolved field, $U^* = \overline{\mathbf{u}}$, and gives this formulation the advective character.

Lastly, the switch ξ only purpose is to guarantee that the force $\mathbf{f}_{\mathrm{SGS}}$ is only present when the detected mode is really the smallest mode the mesh can represent, or in other words, the cut-off mode. Therefore, it guarantees a great selectiveness in frequency, since this force is zero for any other mode with wavelength higher than two mesh spacings.

This concept is easily implemented in a Finite Volume Method framework, as shown in Sampaio et al. (2008) and Sampaio (2006), and it is generally applicable to any unstructured or structured mesh.

NUMERICAL SET-UP

Figure 3 shows the computational domain used throughout this work. The wingspan, L_z, perpendicular to the plane shown in Fig. 3, was one quarter of the chord, c.

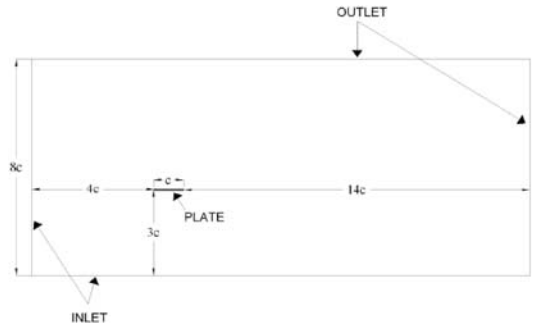

Figure 3: Computational domain.

The mesh employed consisted of 2.5 millions control volumes, with 16 uniformly spaced subdivisions in the spanwise direction. The resulting y^+ was lower than one all over the plate surface, where the maximum aspect ratio was 100. The maximum mesh expansion rate was kept below 1% in the region around the plate, while in the rest of the computational domain, away from the plate, a value of 5% was allowed.

To determine the computational domain size, so that the proximity of the boundaries did not influence the region of interest, several tests were performed. The simple RANS models were employed to speed up the process, since the accuracy of the representation of the turbulence structures were not critical in the determination of the influence of distance between the plate and the boundaries. On the other hand, the same would not be the case for the determination of the mesh spacings, since in this case, the choice of the models has direct impact in the definition of the most appropriate mesh. Therefore, the mesh studies involved a traditional one-Equation subgrid model (Horiuti, 1993) as well as the new proposal based on an advective subgrid forcing term (presented in the previous section, and referred to as "f-LES"), with dynamic-like behavior.

The one-Equation subgrid model did provide, even for the coarser mesh (3-D, with 400 thousands of control volumes, and $y^+ < 8$), better results than the RANS simulations with a very fine 2-D mesh, for which the requirements of $y^+ < 1$ were satisfied everywhere over the plate. However, the results from the one-Equation model with this coarse mesh were not satisfactory due to the lack of an automatic adjustment of the damping effect on the small structures. Too much smoothing was observed even for the mean velocity profiles, leading to the conclusion than too much damping was present. On the other hand, the new proposal (f-LES) provided much better results with the same coarse mesh, and showed clear indications that it indeed have a dynamic-like behavior, similar to the dynamic approach of Germano (1991).

The boundary conditions consist of fixed velocity at inlets ($U_{inlet} = U_\infty = (9.99847, 0.17452, 0)$), and at the plate surface ($U_{plate} = 0$), fixed pressure at outlets ($p_{outlet} = 0$), and zero gradients for pressure at the plate and at inlets, and for velocity at outlets. To mimic the statistically 2-dimensional flow, an "infinity wingspan" was represented through cyclic conditions for all fields at the parallel front and back planes in the wingspan direction. No inlet turbulence was prescribed at inlets, so that very low diffusivity on the numerical schemes was required in order to allow the development of the numerical turbulence throughout the domain.

The Reynolds number for this test case is the same of the experiments of Crompton ($Re = 2.13 \times 10^5$), and the angle of attack was set to 1 degree.

The results for the Dynamic Smagorinsky model were obtained with the commercial software Fluent, while the new proposal was implemented and ran on the opensource code OpenFOAM (www.openfoam.org). Both codes are based on the Finite Volume Method, with fields stored at control volume centroids and interpolated to the faces whenever necessary. Very low-diffusivity numerical schemes were chosen in both cases: bounded central differences scheme in Fluent (almost second order), and pure central differences in OpenFOAM (second order). In this latter case, all energy damping is left to the subgrid model, which is not the case in the former, since boundness can only be guaranteed through a dissipation, even if very small. In order to keep spurious dissipations to a minimum, small time steps (Courant number less than 0.25) and a second order backward difference scheme was the choice for the time discretization. The velocity–pressure coupling is achieved with the PISO (Issa, 1985) algorithm.

In order to speed up the statistical convergence, the starting field for all Large-Eddy Simulations was obtained from a simpler RANS simulation. The final statistics were collected only after convergence to turbulence steady state was observed, with subsequently resetting of all averages.

RESULTS

In this section, results obtained with both subgrid modeling approaches are compared to the first and second order statistics available in Crompton (2001). The traditional Dynamic model is designated as "Dyn" in all graphic legends and tables, while the new approach is referred to as "f-LES". In this latter case, the results for two mesh sizes are presented: "f-LES A" corresponds to the fine mesh of 2.5 thousands (2500k) control volumes, as employed with the Dynamic Model, while "f-LES B" refers to a very coarse mesh (400 thousands), which was obtained with an improved version of the model, where an automatic adjustment of switch ξ parameter was implemented. The purpose of presenting these simulations was just to give an idea of the potential of the "f-LES" approach, which even with a coarse mesh presents reasonable results. The experimental data from Crompton (2001) was designated as "Exp" in all graphs and tables.

General flow characteristics observed in numerical simulations

Due to the abrupt geometry at the main extremity, a long and thin recirculation zone (bubble) is created at the leading edged just after the separation of the boundary layer. If the inclination angle is positive, the stagnation point will be located below the surface of the plate and due to the high inertial forces (high Reynolds number) the particles do not follow the abrupt curvature of the extremity and separation occurs. The separated shear layer is unstable and transition rapidly occurs. After transition, a rapid development of the shear layer occurs due the high rate of turbulence entrainment, which bends the streamlines toward the surface of the plate at the reattachment point X_R. Now, due to the favorable pressure gradient existent between the larger pressure point in the reattachment point and the minimum pressure point close to the bubble center, the portion of the flow that goes back to the leading edge suffers a relaminarization process. The boundary layer of this portion of the flow moves forward to the leading edge becoming again laminar and ready to suffer a second separation, generating a secondary recirculation bubble, since there is another adverse pressure gradient at the minimum pressure point in the center of the bubble to the leading edge. This second very small bubble is very hard to be predicted, and it was not captured by any RANS models. All LES approaches tested in this work were able to capture the flow behavior described above, including the secondary bubble missed by RANS methodology.

Figure 4 shows a side view of the plate with the coherent structures according to the Q criteria. There are two clearly distinct regions: the top turbulent zone corresponds to the outer shear layer, which is part of the main bubble; a smaller region of high turbulence levels, but not as high as this external one, is found inside this top turbulent zone, close to the plate, and corresponds to the secondary recirculation bubble. From the direction of increasing entropy, one can see that the top region develops from left to right, while the inside structures develop from right to left, following the backward flow. Also it is interesting to note how long the shear layer took to transition to turbulence in the top turbulent zone, close to the leading edge. Certainly, for higher Reynolds numbers, the transition point would be much closer to the leading edge, but apparently this delay in transition was still small enough to make the solution accurate and Reynolds number independent. According to experimental data (Crompton, 2001) the flow becomes Reynolds number independent for $Re > 1 \times 10^5$.

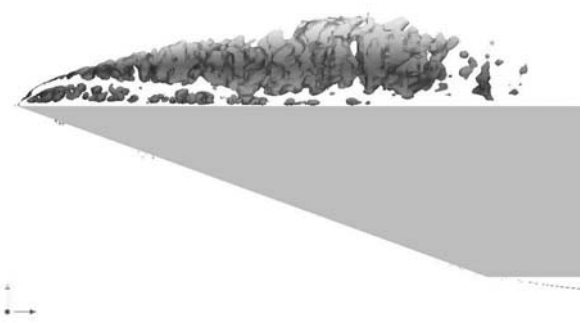

Figure 4: Coherent structures according to Q criteria.

First order statistics

The numerical prediction of the mean reattachment lengths (X_R) obtained with the different turbulence models are presented in Table 1.

Table 1: Reattachment lengths.

	Exp	Dyn	f-LES A	f-LES B
X_R/c	0.14	0.1409	0.1269	0.1359
Error (%)	–	0.642	9.4	3

The accuracy of the prediction of the reattachment lengths for this flow under investigation is believed to be influenced by several factors, including the correct prediction of the stagnation point under the plate, and the correct prescription of the inlet turbulence intensity. The former is directly dependent on the mesh size, while the latter was set to zero in this study, for the sake of simplicity. Another factor that is believed to influence the resulting bubble length is the control volumes aspect ratio. Therefore this parameter alone should not be taken as ultimately conclusive when comparing the different models. Having said that, it is clear from Table 1 that the Dynamic model indeed provided the most accurate result in this respect, and that the "f-LES" with the coarse mesh also presented a better prediction when compared to the original advective formulation.

Crompton (2001) made available the data for the mean velocity and turbulent fluctuations at four stations normal to the plate, located at $x/c = 0.03125$, $x/c = 0.125$, $x/c = 0.25$, and $x/c = 0.375$. Notice that, according to Table 1, the first two of these stations are located inside the leading edge recirculation bubble, while the last two stations are outside this region, in a development zone. Also it is worth noting that the second of these stations is situated at the very end of the bubble, almost outside.

The same four stations chosen by Crompton are used to compare the velocity and turbulence results obtained with the experimental data.

Due to the strong sensitivity of reattachment length in respect to several aspects of the simulation, as mentioned above, it is common practice in the literature to correct the normalized distance along the plate, x/c, with the ratio between the numerically obtained reattachment length (X_{RN}) and the experimental one (X_R). This means that the stations are ultimately located at x/c, with cX_{RN}/X_R substituting c henceforth. With this correction, the ability of a certain model to correctly capture the flow development is isolated from its ability to capture the recirculation bubble, and it might happen that one model is less accurate for X_R, but apart from that, is the most accurate in predicting how the flow develops in the streamwise direction. Therefore, to allow a more fair comparison and isolate the different causes of accuracy problems, the results presented here normalized with the corrected cord.

Having said that, the $x-$component of the mean velocity profiles at the four stations along the plate are presented in Fig. 5(a)-(d), normalized by the freestream velocity, U_∞. In general, all LES results were in excellent agreement with the experimental data, specially when compared to previous RANS simulations (Collie, 2008, and Rezende and Nieckele, 2007). This is true even for the very course mesh ("f-LES B"), which was not that much more expensive than the RANS. The development of the profiles, along the plate from station 2, was slightly better captured by the new proposal, even with the course mesh: the Dy-

namic Smagorinsky clearly showed some "smoothing" at station 2, where "f-LES" correctly captured the predominantly "piecewise linear" behavior, with almost perfect accuracy; at stations 3 and 4, the slopes $\partial \langle U_x \rangle / \partial y$ captured by both f-LES simulations were closer to the experimental data, while those captured by the Dynamic Smagorinsky were somewhat underpredicted, specially outside the viscous layer, from $y/c = 0.00625$ to 0.025.

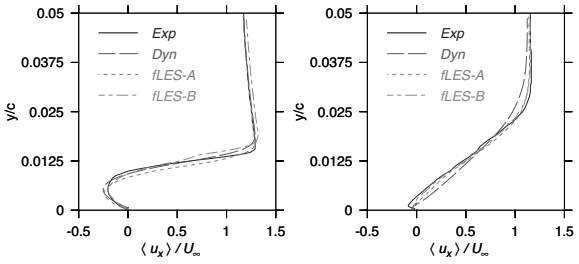

(a) $x/c = 0.03125$ (b) $x/c = 0.125$

(c) $x/c = 0.250$ (d) $x/c = 0.375$

Figure 5: Mean streamwise velocity profiles, at: (a) $x/c = 0.03125$; (b) $x/c = 0.125$; (c) $x/c = 0.250$; (d) $x/c = 0.375$.

The pressure coefficient, $cp = (p - p_\infty) / \left(0.5 U_\infty^2\right)$, along the plate upper surface, is plotted against the normalized distance x/c in Fig. 6, where it can be seen that all models reproduced remarkably well the experimental data. The only exception is the case with the very coarse mesh: to keep the number of control volumes down, a high rate stretching was used as the trailing edge is approached. That explains the discrepancy found toward the end of the plate in the "f-LES B" case.

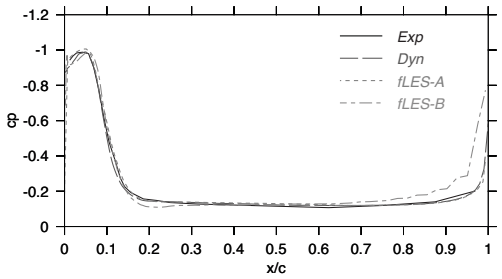

Figure 6: Pressure coefficient along the plate.

Second order statistics

The profiles of turbulent fluctuations in the streamwise direction, $\langle u'u' \rangle$ are shown normalized by the square of the freestream velocity, U_∞, in Fig. 7(a)-(d). These fluctuations are in fact time averages of the resolved fluctuations around the time average mean velocity. Therefore, it does not include the subgrid part and as such, it is not expected to accurately reproduce the experimental Reynolds fluctuation, plotted in the same Figure. However, as mesh gets finer and approaches DNS, the numerical fluctuations should approach both the experimental data and DNS results. Indeed, one can see that the coarse mesh used in the "f-LES B" simulations always underpredicted the fluctuations intensity. That means that even missing some important part of the energetic structures, f-LES could still get the first order statistics quite right, with considerable advantages over RANS methodology. On the other hand, it is clear that both approaches (Dyn and f-LES), with the refined mesh, present more or less the same accuracy, with a small advantage to the new proposal ("f-LES A") in the last two stations.

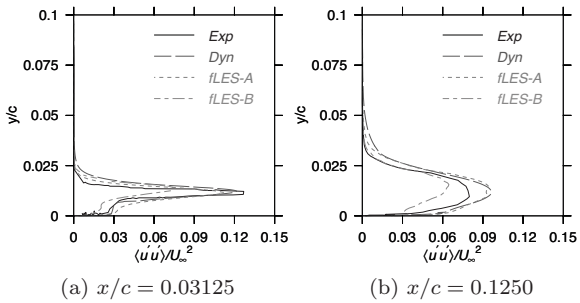

(a) $x/c = 0.03125$ (b) $x/c = 0.1250$

(c) $x/c = 0.250$ (d) $x/c = 0.375$

Figure 7: Turbulent fluctuations at: (a) $x/c = 0.03125$; (b) $x/c = 0.125$; (c) $x/c = 0.250$; (d) $x/c = 0.375$.

In general, the evolution of turbulence in the streamwise direction, corresponding to the sequence of Fig. 7(a) to (d), is well captured by all simulations. A quick transition to turbulence in the separated shear layer, immediately after leading edge separation, result in the high and sharp pick apparent at station 1, close to 12% (or 35% rms), located at $y/c = 0.0125$. It is clear that the mesh in this region was fine enough (in the Dyn and f-LES A cases) to accurately capture this transition. Downstream, this concentrated turbulent energy begins to spread, subsequently lowering the pick value and widening the turbulence zone away from the wall as we pass through stations 2, 3, and 4, in a clearly diffusive process. The fact that the turbulence levels at station 2 were overpredicted is an indication that, for some reason, the turbulence diffusion process was slower than it should, or that the numerical generation of turbulence was still too high between stations 1 and 2.

FINAL REMARKS

Two different approaches to subgrid modeling in Large-Edge Simulations were tested for the highly anisotropic turbulent flow around a thin flat plate at small incidence. One of them, the traditional Dynamic Smagorinsky model, was based on an eddy-viscosity hypothesis, while the other, a new proposal, was based on an advective forcing formulation. The objective of this new proposal was to test if the

generally accepted Boussinesq hypothesis was really a strong requirement, and to understand the interaction of turbulence modeling with numerical schemes. Two meshes, one extremely coarse and one sufficiently refined and suitable to LES at the target Re number were also tested.

Regarding the tests on the finer mesh, one can conclude from the results that some of the flow features were better captured by the new proposal proposal, specially regarding the flow development in the streamwise direction. The mean velocity profiles were in better agreement with the experimental data, while the corresponding Dynamic results were somewhat smeared out, probably by some spurious dissipation. Most likely, this dissipation did not come from the subgrid model itself, but probably from the additional stability employed in the numerical schemes of the commercial code (bounded central differences instead of purely central differences). In the new proposal, all dissipation is left to the physical model, where the smallest modes still representable by the mesh are damped according to some very frequency selective criteria, based on physical arguments.

On the other hand, the Dynamic model predicted a much more accurate reattachment length, although this alone is not very conclusive.

The finer mesh was proved adequate to this study, which can be seen by the turbulent fluctuations profiles that clearly indicated that most of the energy was well represented. The same cannot be said about the coarser mesh, even though it was still good to capture the first order statistics and the general flow behavior, providing a significant advantage over RANS methodology, with an affordable increase in the computational cost.

ACKNOWLEDGEMENT

The authors gratefully acknowledge the support awarded to this research by the Brazilian Research Council - CNPq.

REFERENCES

Collie, S.; Gerritsen, M.; Jackson, P., 2008, "Performance of Two-equation Turbulence Models for Flat Plate Flows with Leading Edge Bubbles", *Journal of Fluids Engineering-Transactions of the ASME*, Vol. 130:2, Article Number: 021201.

Crompton, M., 2001, *The Thin Airfoil Leading Edge Separation Bubble*, PhD Thesis, Department of Aerospace Engineering University of Bristol.

Cyr, S. and Newman, B. G., 1996, "Flow past two-dimensional membrane aerofoils with rear separation", *Journal Of Wind Engineering And Industrial Aerodynamics*, Vol. 63:1-3, pp. 1-16.

Gault, D. E., 1957, "An investigation at low speed of the flow over a flat plate at small angles of attack using pitot static and hot-wire probes", *Technical Report TN-3876*, NACA.

Germano, M.; Piomelli, U.; Moin, P. and Cabot, W. H., 1991, "A dynamic subgrid-scale eddy viscosity model", *Physics of Fluids A*, Vol. 3:7, pp. 1760-1765.

Germano, M., 1999, "From RANS to DNS: Towards a Bridging Model", *Direct and Large-Eddy Simulation III, Proceedings of the Isaac Newton Institute Symposium / ERCOFTAC workshop*, Vol. 7, pp. 225-236, Kluwer.

Horiuti, K., 1989, "The role of the Bardina model in large eddy simulation of turbulent channel flow", *Physics of Fluids A - Fluid Dynamics* , Vol 1:2, pp 426-428.

Horiuti, K., 1993, "A Proper Velocity Scale for Modeling Subgrid-Scale Eddy Viscosities in Large Eddy Simulation", *Physics of Fluids A - Fluid Dynamics*, Vol. 5:1, pp. 146-157.

Issa, R., 1998, "Solution of the Implicit Discretized Fluid Flow Equations by Operator-Splitting", *Journal of Computational Physics*, Vol. 62, pp. 40 - 65.

Lian, Y. S. and Shyy, W., 2005, "Numerical simulations of membrane wing aerodynamics for micro air vehicle applications", *Journal Of Aircraft*, Vol. 42:4, pp. 865-873.

Newman, B. G. and Tse, M. C., 1992, "Incompressible-Flow Past A Flat-Plate Aerofoil With Leading-Edge Separation Bubble", *Aeronautical Journal*, Vol. 96:952, pp. 57-64.

Rezende, A. L. T. and Nieckele, A. O., 2007, "Prediction of the Flow Over a Thin Flat Plate at Shallow Incidence", *Proceedings of the 19th International Congress of Mechanical Engineering - COBEM 2007*, Brasılia, BR, Article number: 433.

Sagaut, P., 2002, *Large Eddy Simulation for Incompressible Flows, An Introduction*, Springer, Berlin Heidelberg New York, Second Edition.

Sampaio, L. E. B., 2006, *Large Eddy Simulations of the Thin Plate Separation Bubble at Shallow Incidence*, DSc. Thesis, Department of Mechanical Engineering, Pontifícia Universidade Católica do Rio de Janeiro, RJ, Brasil, in Portuguese.

Sampaio, L. E. B.; Nieckele, A. O. and Gerritsen, M., 2008, *Performance assessment of a new advective subgrid model through two classic benchmark test cases*, Quality and Reliability of Large-Eddy Simulations, Editors J. Meyers, J; Geurts, B. and Sagaut, P.; Ercoftac Series, Springer, Vol. 12, pp. 283-294.

Smagorinsky, J., 1963, "General circulation experiments with the primitive equations. I: the basic experiment", *Monthly Weather*, Vol. Rev. 91:3, pp. 99-165.